

Electronic Supplementary Information (ESI):

**Exploring the Electrochemical Performance of Graphite
and Graphene Paste Electrodes Composed of Varying
Lateral Flake Sizes**

Anthony J. Slate^{1,2}, Dale A. C. Brownson^{1,2*}, Ahmed S. Abo Dena^{3,4},
Graham C. Smith⁵, Kathryn A. Whitehead¹ and Craig E. Banks^{1,2*}

*¹: Faculty of Science and Engineering, Manchester Metropolitan University,
Chester Street, Manchester, M1 5GD, UK.*

*²: Manchester Fuel Cell Innovation Centre, Manchester Metropolitan University, Chester
Street, Manchester M1 5GD, UK.*

*³: Faculty of Oral and Dental Medicine, Future University in Egypt (FUE), New Cairo,
Egypt.*

*⁴: National Organization for Drug Control and Research (NODCAR), Giza, P.O. Box 29,
Egypt.*

*⁵: Faculty of Science and Engineering, Department of Natural Sciences, University of
Chester, Thornton Science Park, Pool Lane, Ince, Chester CH2 4NU, UK.*

*To whom correspondence should be addressed.

Email: d.brownson@mmu.ac.uk; Tel: ++(0)1612476561

c.banks@mmu.ac.uk; Fax: ++44 (0)1612476831; Tel: ++44 (0)1612471196

Website: www.craigbanksresearch.com

Chemical Composition of the Various Graphene/Graphite Powders

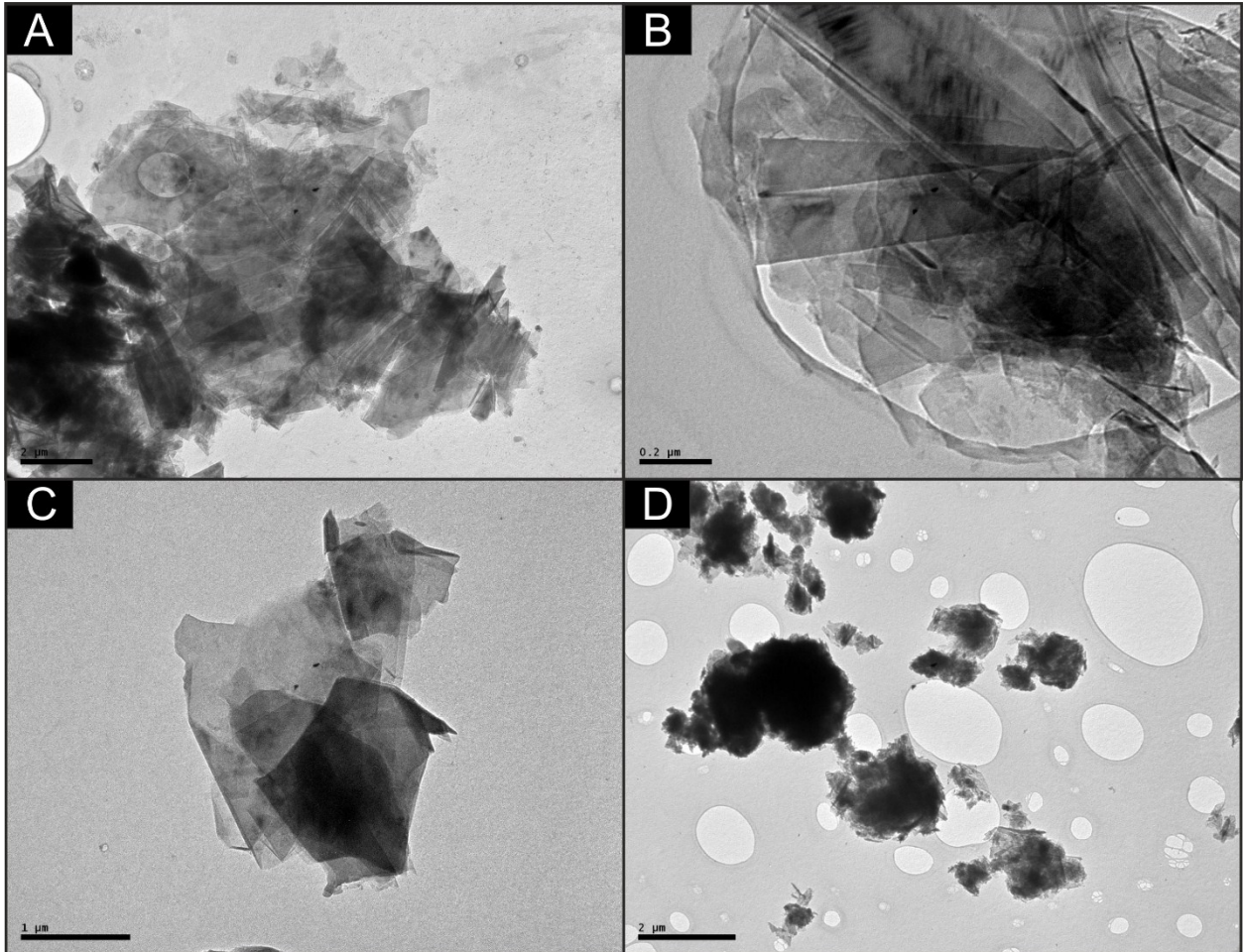
XRD was performed on each of the graphite and graphene powders, with the resulting spectra presented in ESI Figures 12 and 13 respectively. The XRD patterns evident represent the expected characteristic peaks at $2\theta = 26.9^\circ$, 43.7° and 55.2° , corresponding to the (002), (101) and (004) diffraction peaks of graphitic powders and thus confirm the presence of graphene/graphite.¹⁻³ Chemical analysis was also conducted on each of the powders to determine their elemental and specific moiety compositions (if present). EDX analysis (ESI Table 8) details the average atomic percentage (%) in terms of the elemental composition of the various graphite and graphene powders. As expected, the two major components of all samples was on average *ca.* 94.86% atomic carbon and *ca.* 4.28% atomic oxygen, indicating high quality/purity graphitic powders with a small presence of oxygenated species likely. Although trace quantities of other elements were observed, given their insignificantly small % presence/contribution, they are not considered to contribute towards the electro-catalytic activities of the paste electrodes.

XPS was conducted on the range of graphitic powders to further investigate the composition and quantity of any specific moieties and oxygenated species present in each instance (ESI Figures 14 and 15 and ESI Tables 1 and 2). De-convolution of the spectra revealed that on average the powders comprised *ca.* 95.2 % carbon and 3.7 % oxygen. The carbon content corresponds to 284.6 eV, which is characteristic of sp^2 carbon and graphitic groups, with small contributions evident from 286.2 eV and 289.6 eV, which both correspond to C–O and C=O bonds respectively.⁴ The majority of the oxygen content corresponds to a broad feature centred at 531.0 eV, which has a variety of possible origins including absorbed water, but this is most likely indicative of both C–O and C=O groups, with an equal contribution from both bonds (and a small contribution from O=C–O) found through careful de-convolution.^{5,6}

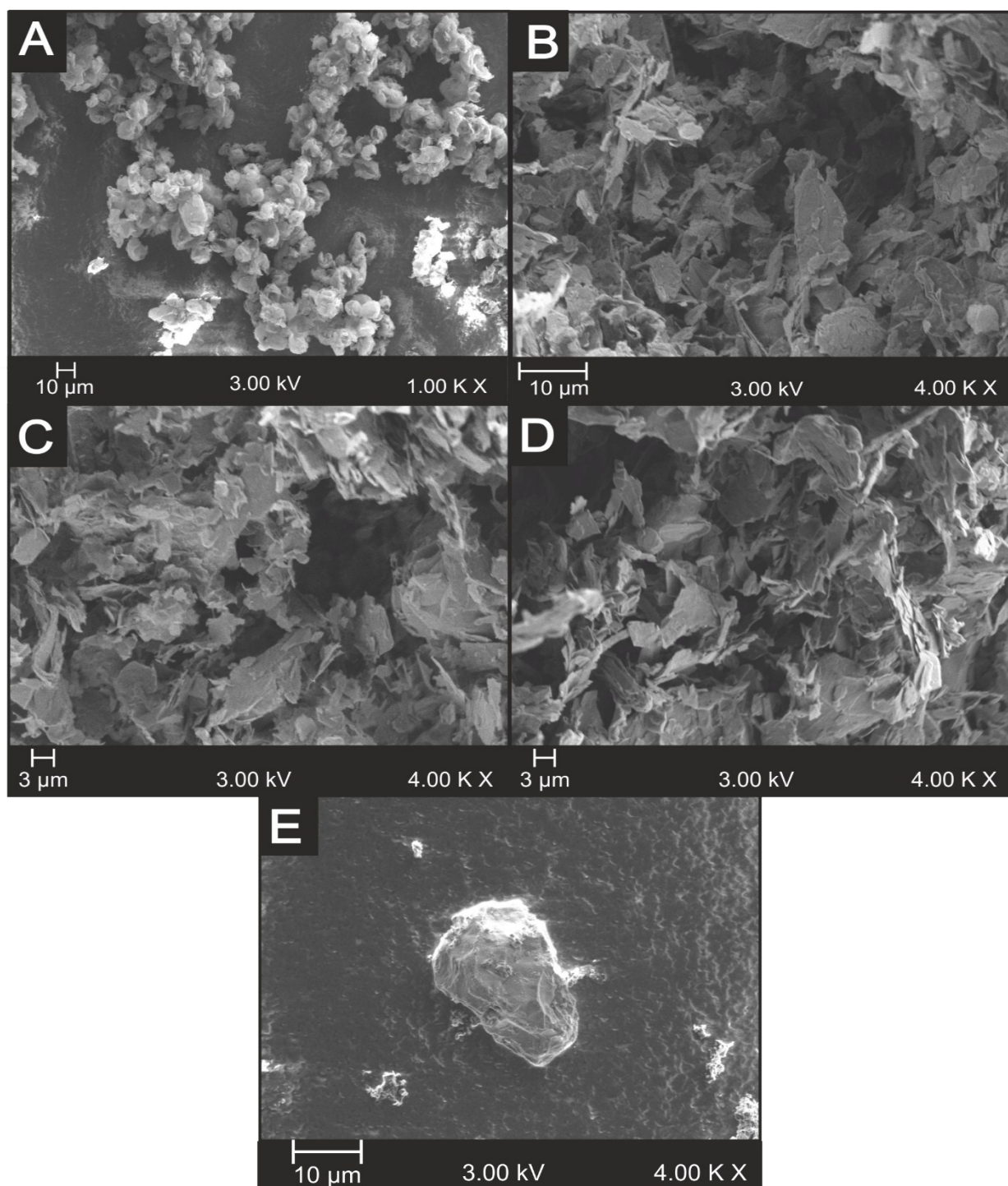
Electrochemical Inner- and Outer- Sphere Redox Probes

Both inner- and outer- sphere electrochemical redox probes were utilised throughout this work. Outer-sphere redox mediators such as Hexaammineruthenium(III) chloride are described as surface insensitive, where the oxygen/carbon ratio on the electrode's surface in addition to any specific surface characteristics (such as surface sites/groups, *i.e.* ligands) do not influence the k^0 values obtained.⁸ In these cases, the electrochemical response observed is dependent only upon the electronic structure of the electrode material (electronic Density of States, DoS) and thus for the case of graphitic materials, the respective coverage of 'reactive' edge plane sites (opposed to the relatively 'un-reactive' basal plane sites), where the electrode acts merely as a source (or sink) of electrons. On the other hand, inner-sphere redox mediators, such as potassium ferrocyanide(II) are deemed surface sensitive, where the k^0 is strongly influenced by the state of the electrode surface. This refers to a variety of factors including both the microstructure and surface chemistry, *via* specific electrocatalytic interactions that can be significantly inhibited by surface obscurities. Inner-sphere redox probes are highly dependent on either the presence or the absence of specific oxygenated species, leading to detrimental or beneficial electrochemical effects.⁸

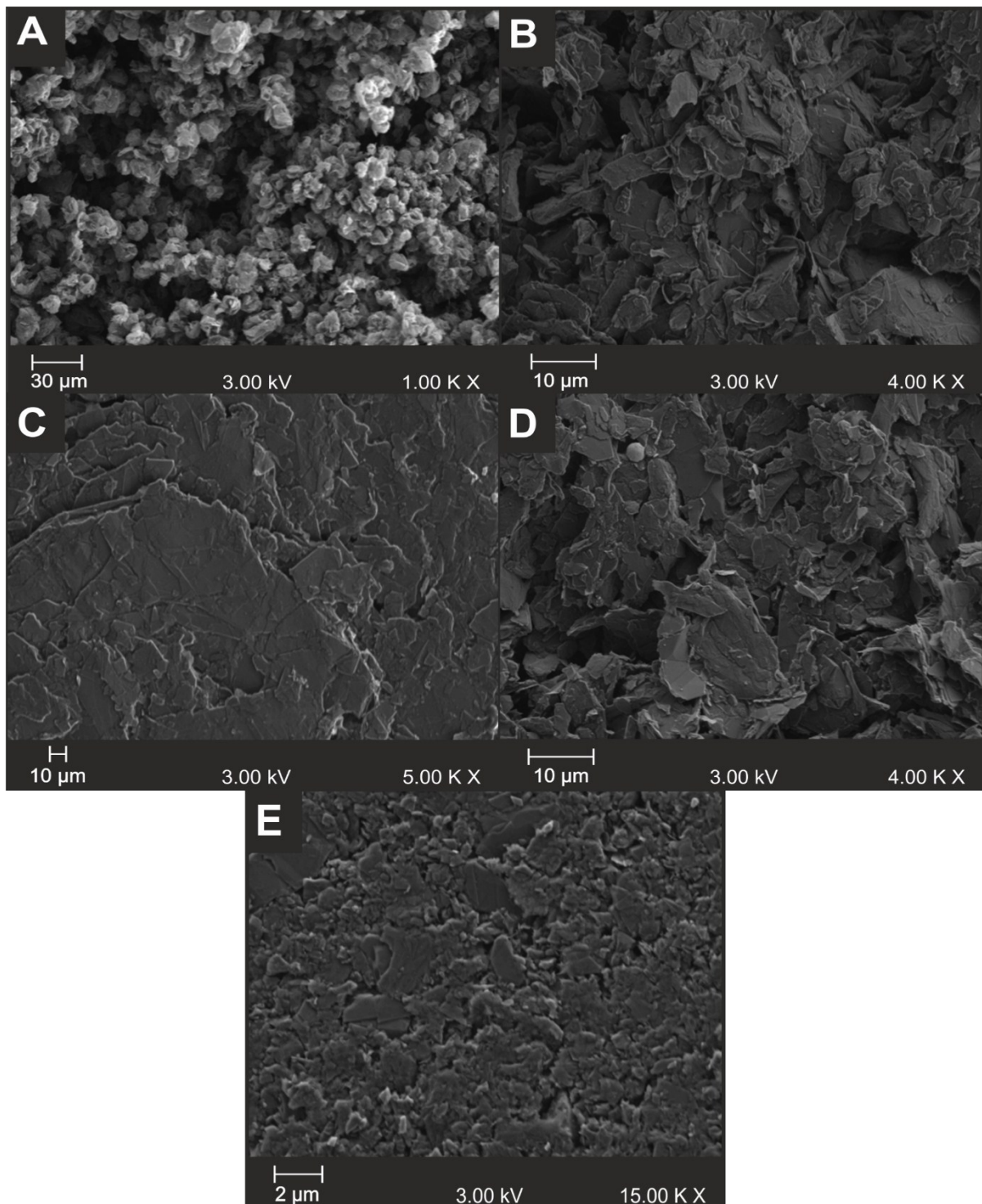
ESI Figure 1. Structural characterisation of the graphite flakes *via* TEM where distinct lateral flake sizes are evident; A) kish graphite (scale bar, 2.0 μm), B) flake graphite (scale bar, 0.2 μm), C) high crystalline natural graphite HCN (scale bar, 1.0 μm), D) nanostructured graphite – 250 (scale bar, 2.0 μm).



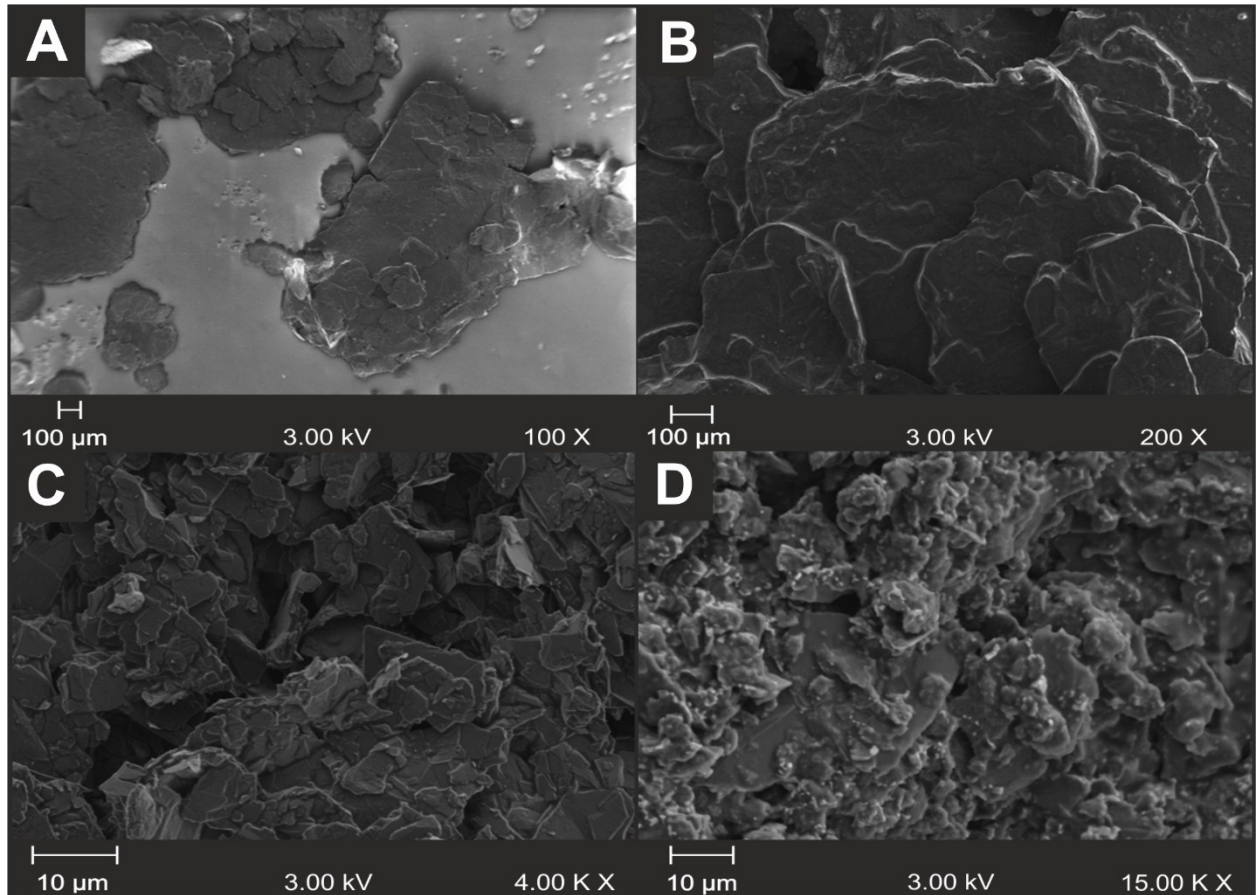
ESI Figure 2. SEM images of the graphene powders used to fabricate the paste electrodes – indicating the carrying lateral flake sizes; A) AO1, B) AO2, C) AO3, D) AO4, and E) C1.



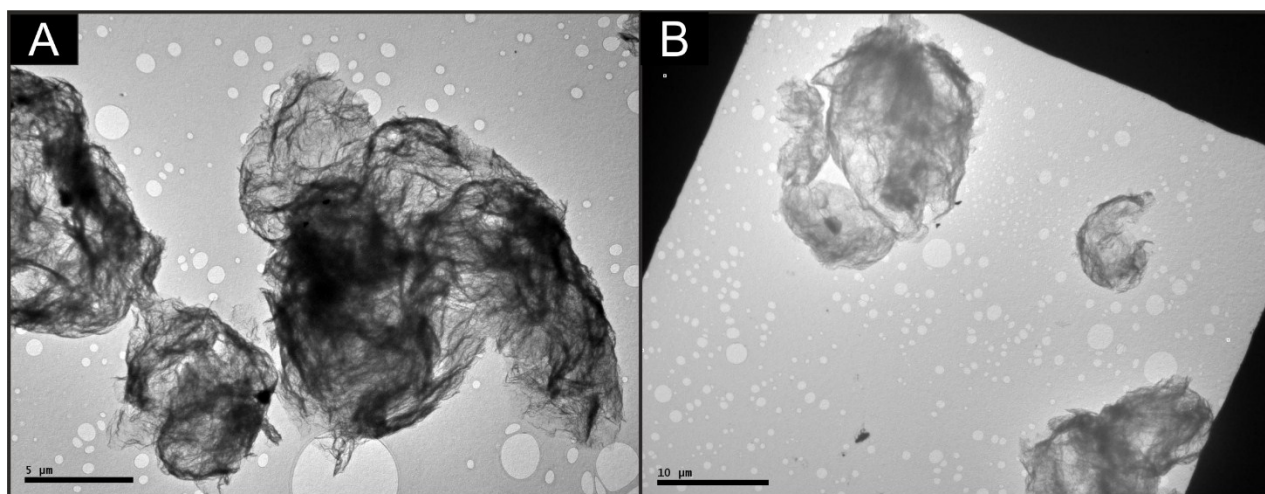
ESI Figure 3. SEM images of the surface of the graphene paste electrodes – showing individual lateral flake sizes; A) AO1, B) AO2, C) AO3, D) AO4, and E) C1.



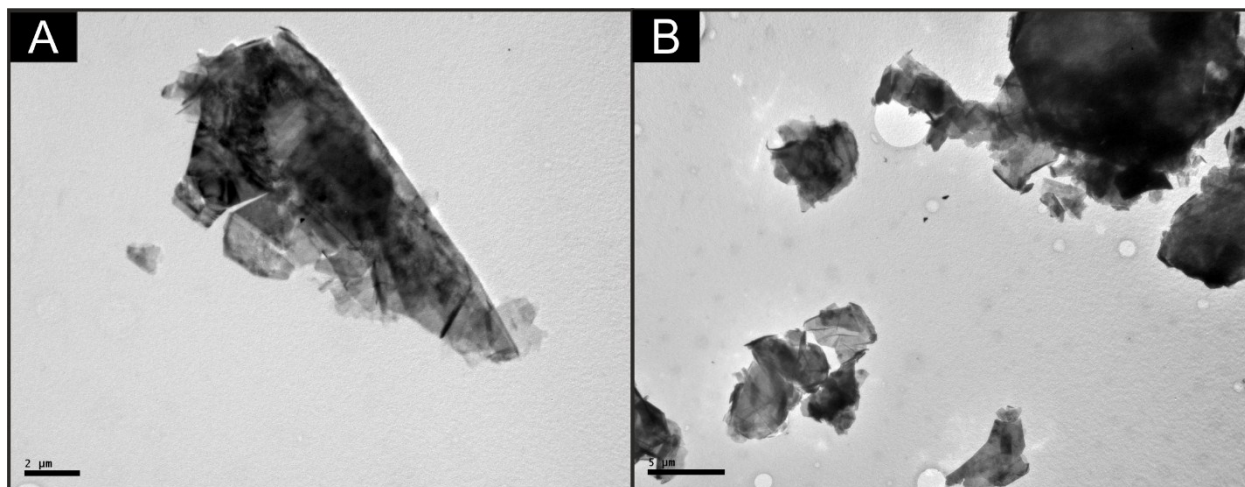
ESI Figure 4. SEM images of the surface of the graphitic paste electrodes – showing individual lateral flake sizes; A) kish graphite, B) flake graphite, C) HCN graphite, and D) nanostructured graphite – 250.



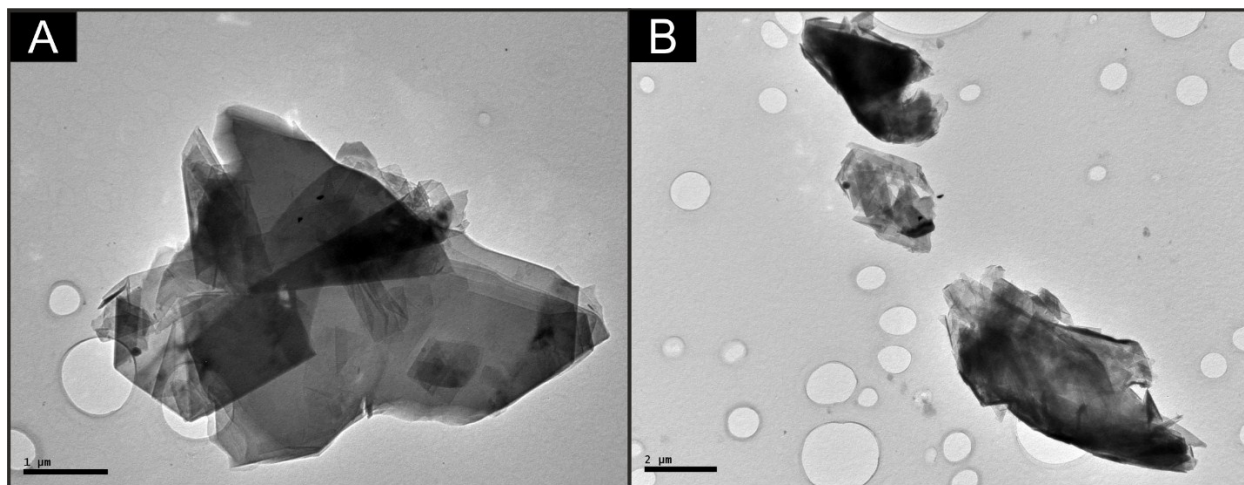
ESI Figure 5. Additional structural characterisation of the graphene lateral flake AO-1, *via* TEM images. Note, the difference in scale A) 5 μm scale bar B) 10 μm scale bar.



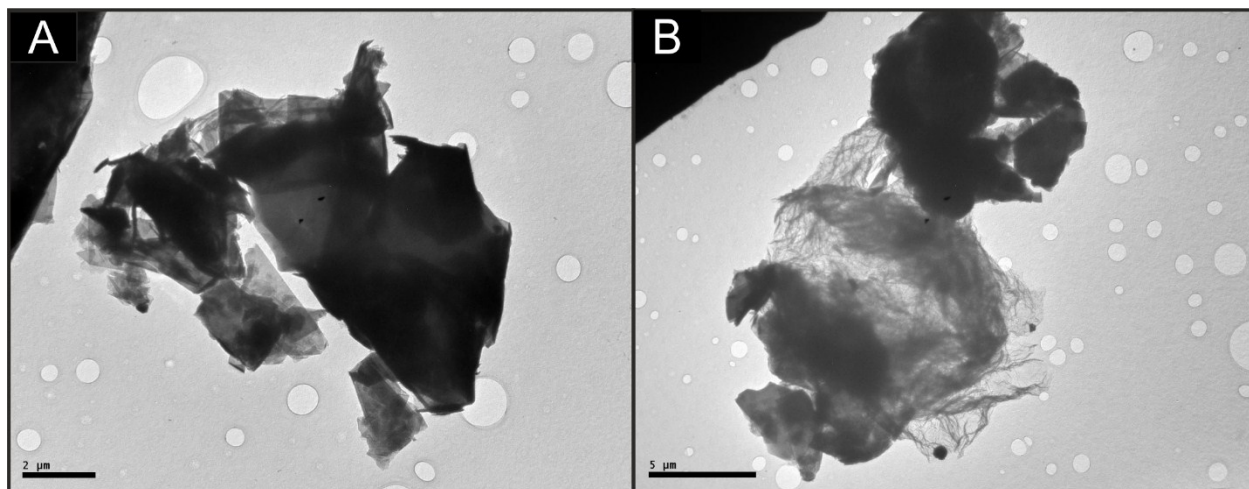
ESI Figure 6. Additional structural characterisation of the graphene lateral flake AO-3, *via* TEM images. Note, the difference in scale A) 2 μm scale bar B) 5 μm scale bar.



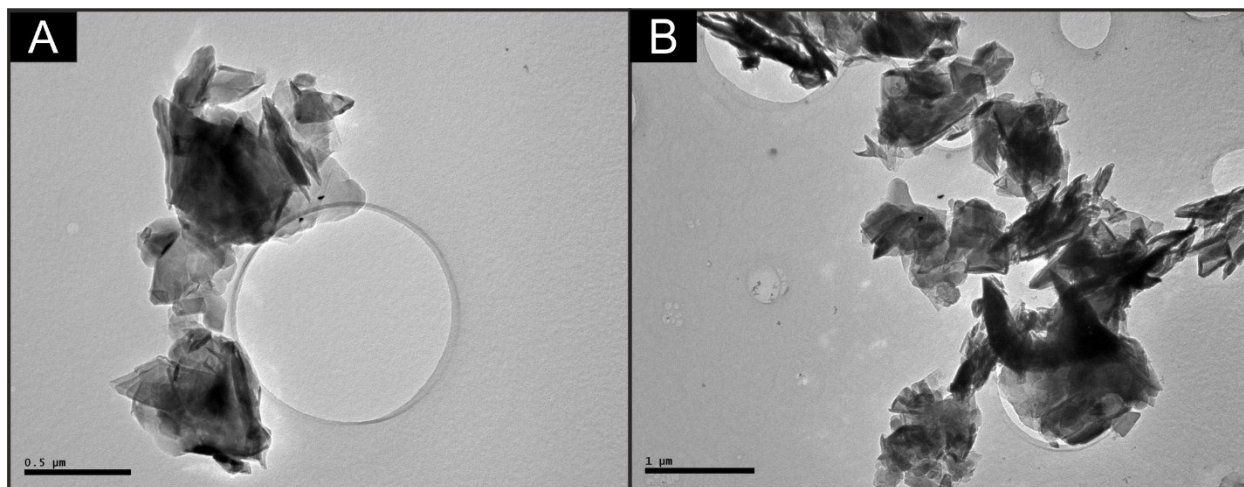
ESI Figure 7. Additional structural characterisation of the graphene lateral flake AO-4, *via* TEM images. Note, the difference in scale A) 1 μm scale bar B) 2 μm scale bar.



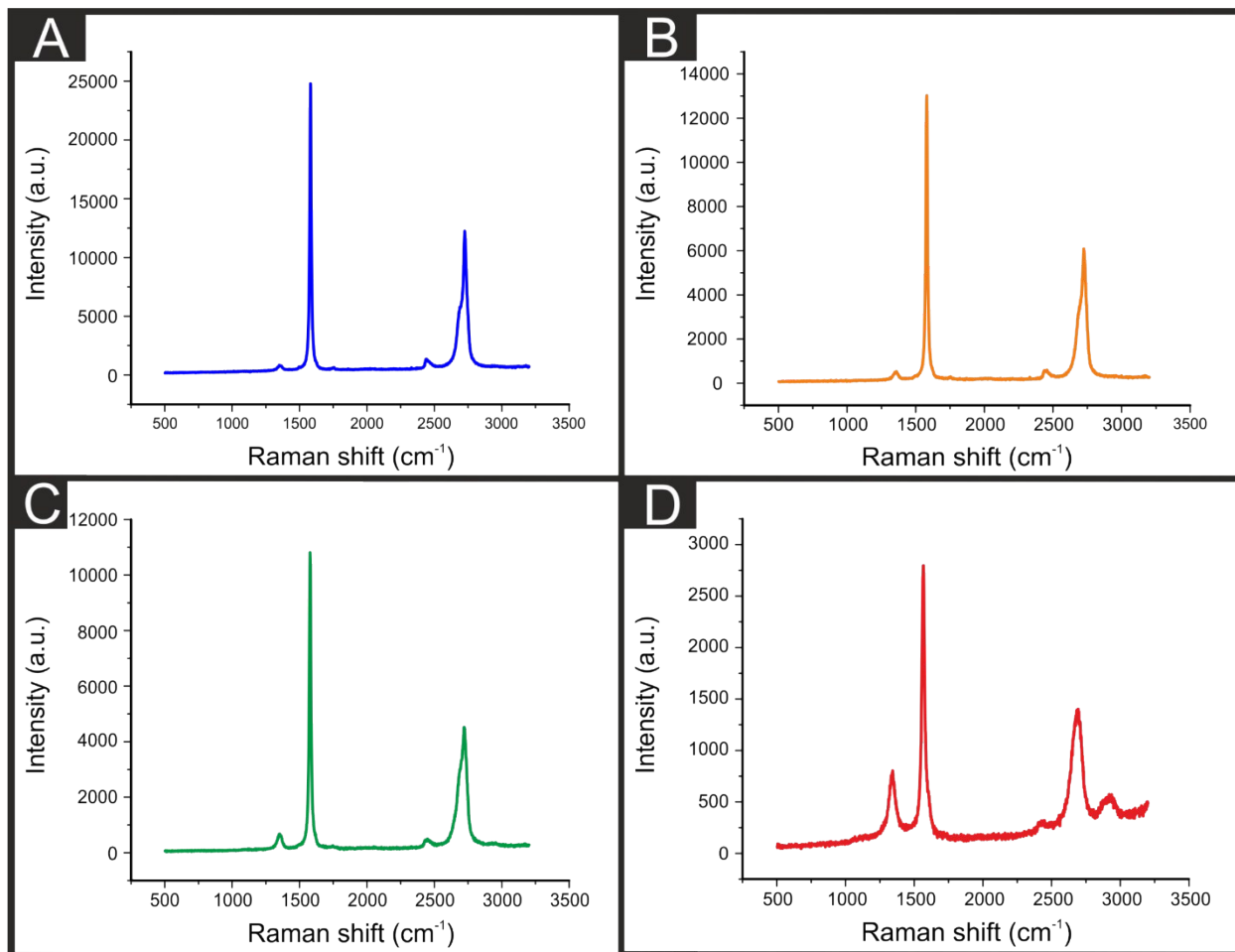
ESI Figure 8 Additional structural characterisation of the graphene lateral flake AO-2, *via* TEM images. Note, the difference in scale A) 2 μm scale bar B) 5 μm scale bar.



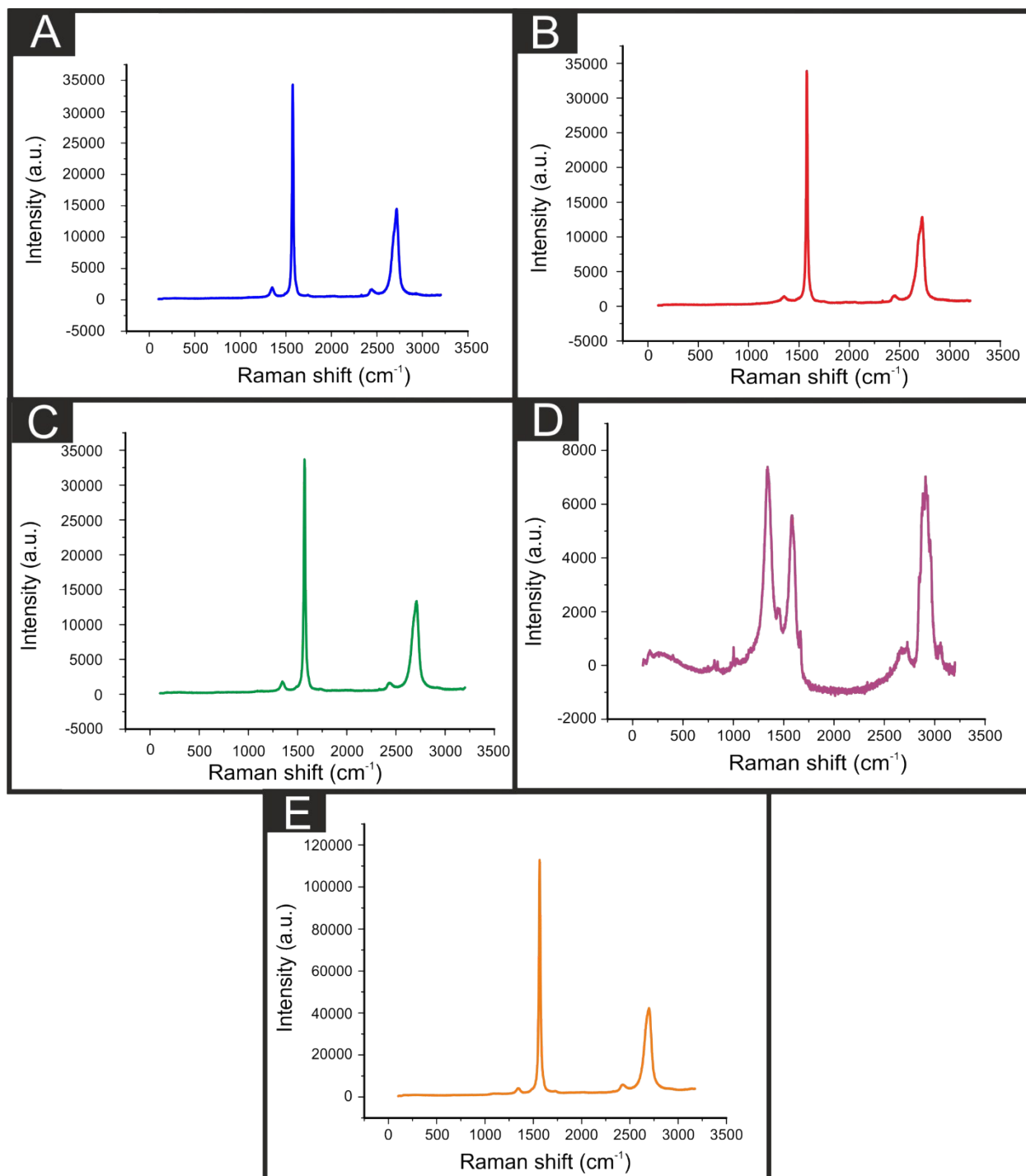
ESI Figure 9. Additional structural characterisation of the graphene lateral flake C1, *via* TEM images. Note, the difference in scale A) 0.5 μm scale bar B) 1.0 μm scale bar.



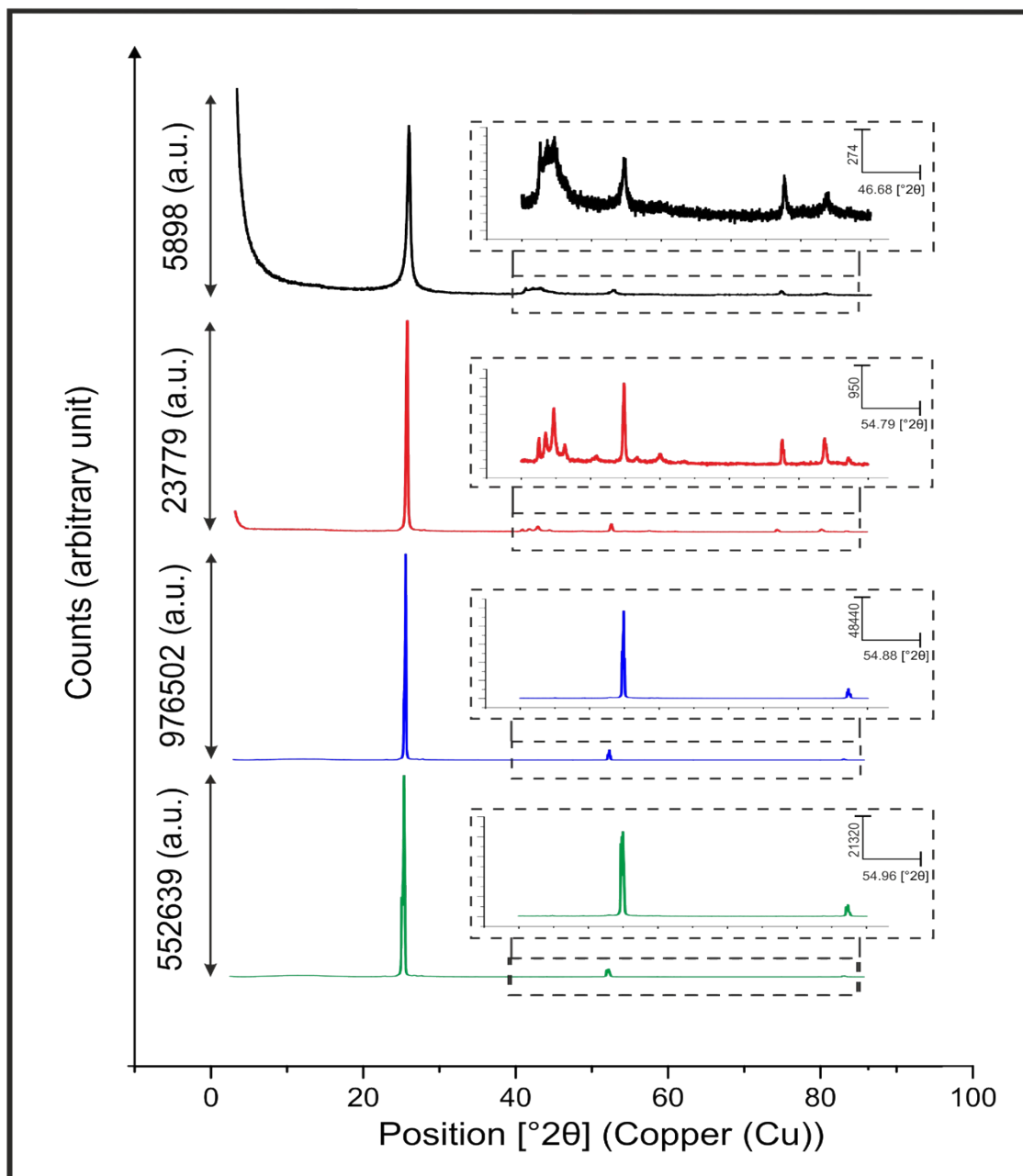
ESI Figure 10. Raman spectra of the four graphitic powders. A) Kish graphite (blue), B) Flake graphite (orange), C) HCN graphite (green), and D) Nanostructured graphite (red). Note the variation in band ratios when the lateral flake size decreases and the emergence of the edge plane/defect band at *ca.* 1300 cm^{-1} .



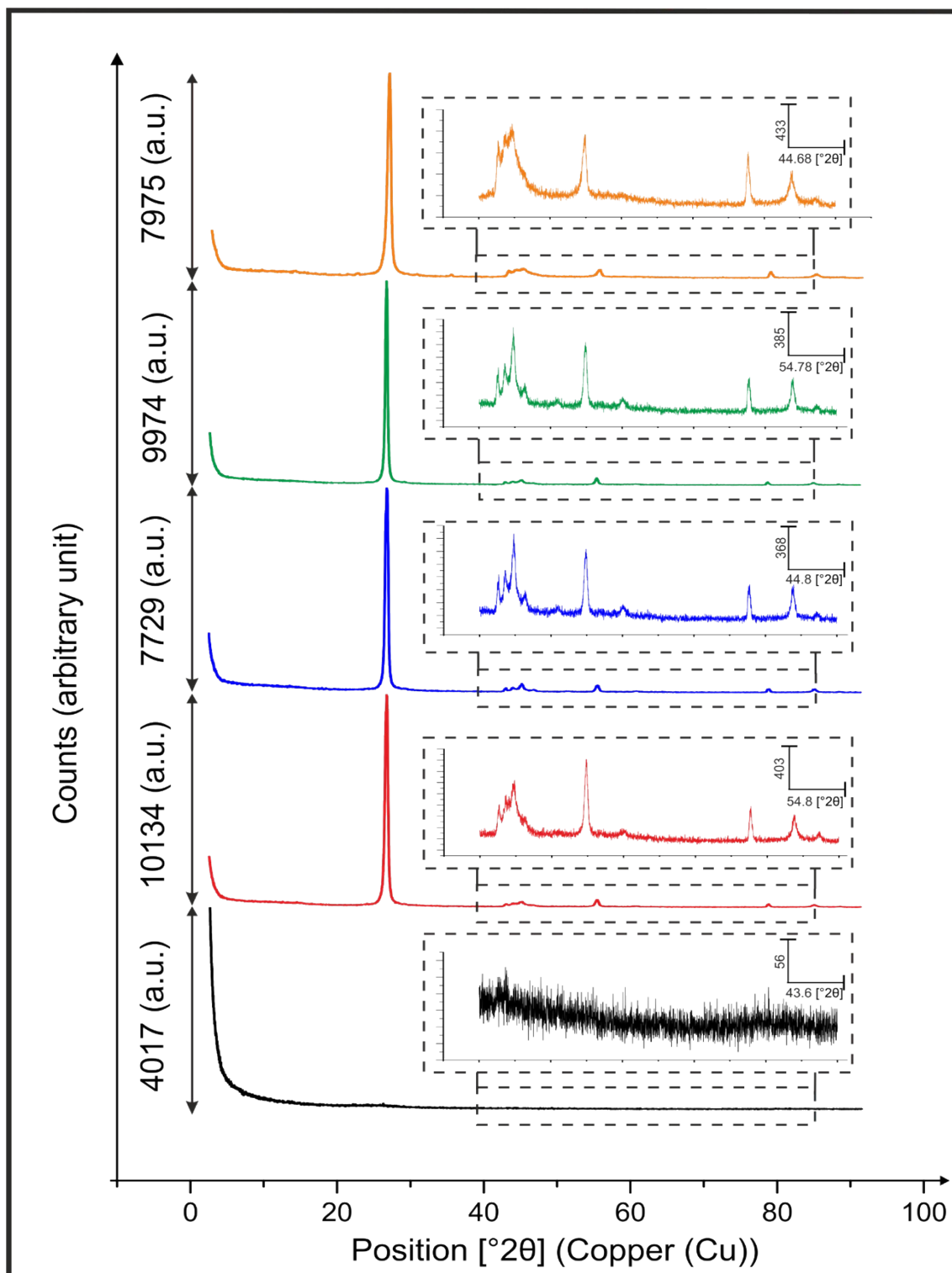
ESI Figure 11. Raman spectra of the five graphene powders. A) AO-2, B) AO-3, C) AO-4, D) AO-1, and E) C1.



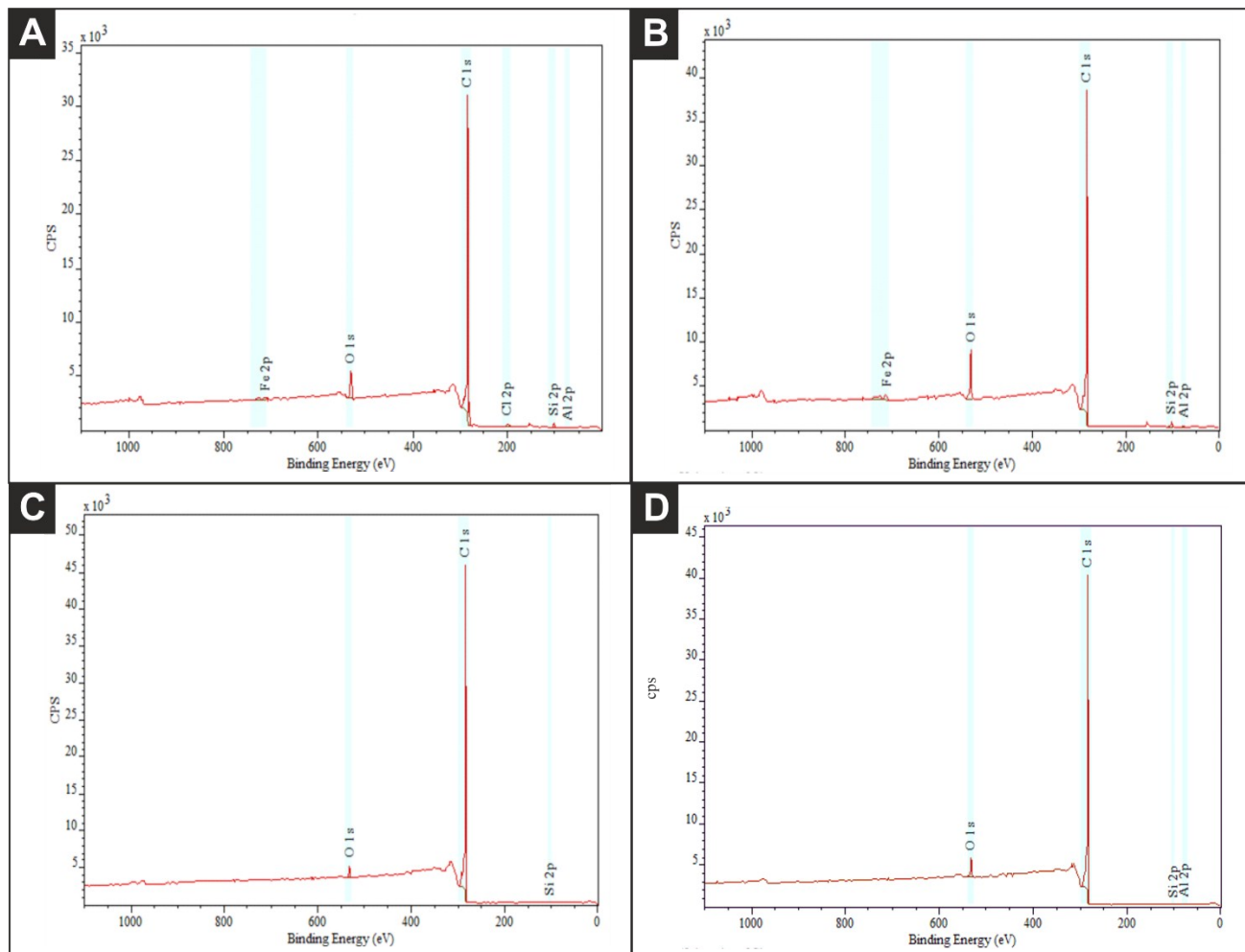
ESI Figure 12. XRD spectra showing the carbon peaks of the commercially procured graphite powders, following deposition onto a glass slide. Position [$^{\circ}2\theta$] (Copper (Cu)). The black line denotes, nanostructured graphite – 250, the red line – high crystalline natural (HCN) graphite, the blue line – flake graphite and the green line – kish graphite. Note, the inset on each spectra shows an enlarged scale of the region indicated.



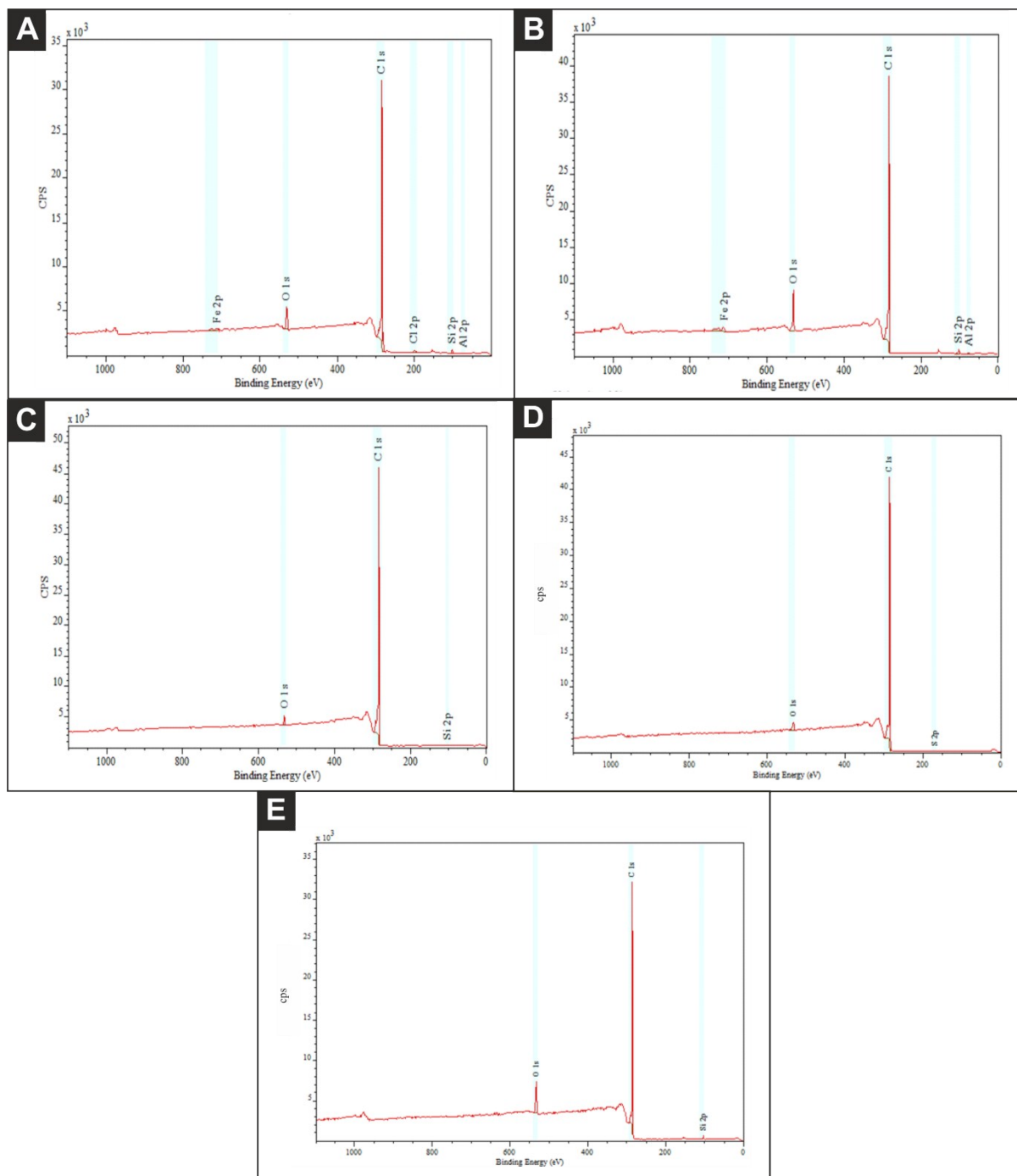
ESI Figure 13. XRD spectra showing the carbon peaks of the commercially procured graphene powders, deposited onto a glass slide. Position [$^{\circ}2\theta$] (Copper (Cu)). The black line denotes – AO1, the red line AO2, the blue line – AO3, the green line – AO4 and the orange line – C1. Note, the inset on each spectra shows an enlarged scale of the region indicated.



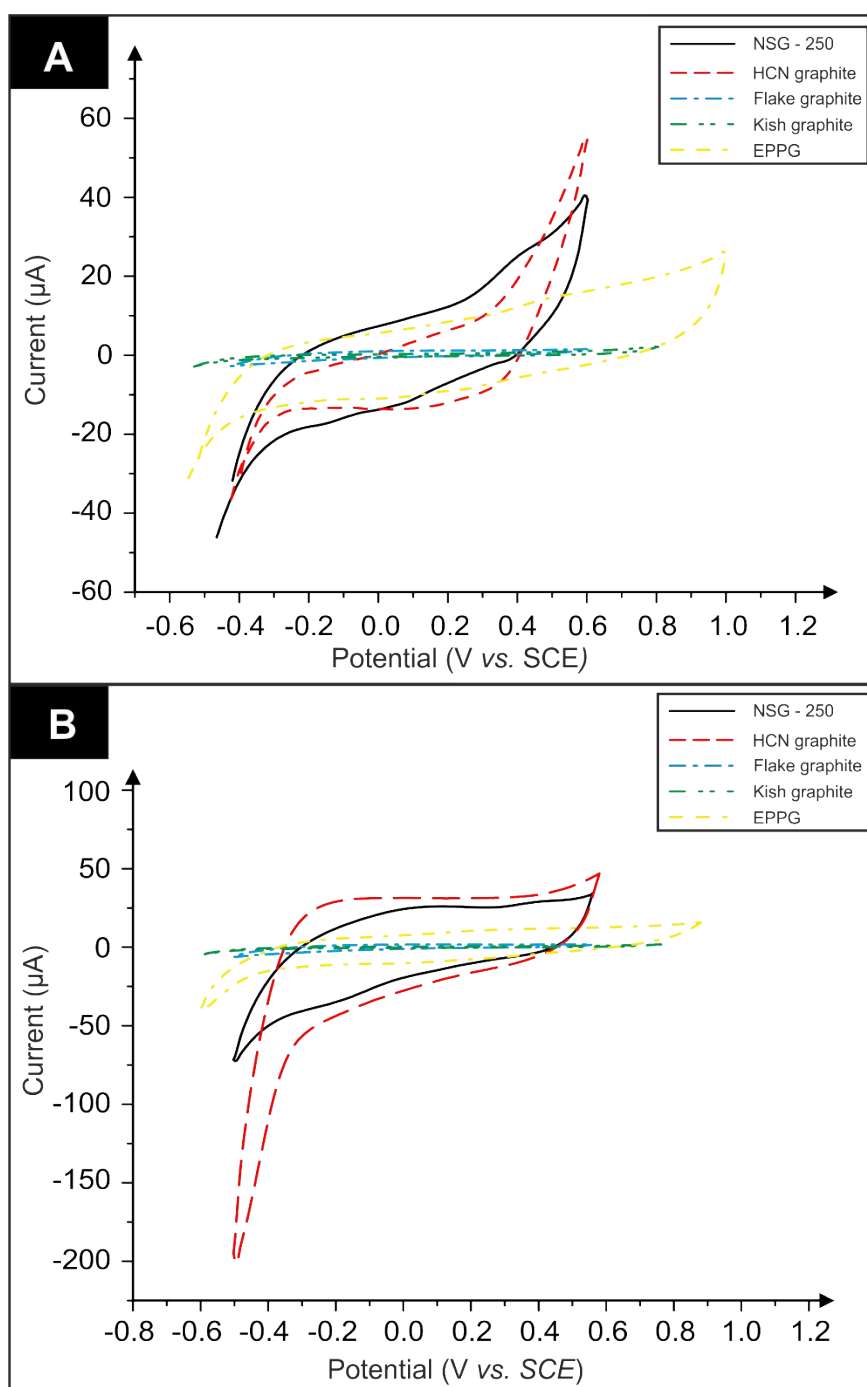
ESI Figure 14. XPS spectra showing the typical carbon responses of the commercially procured graphite powders; A) kish graphite, B) flake graphite, C) high crystalline natural graphite and D) nanostructured graphite – 250.



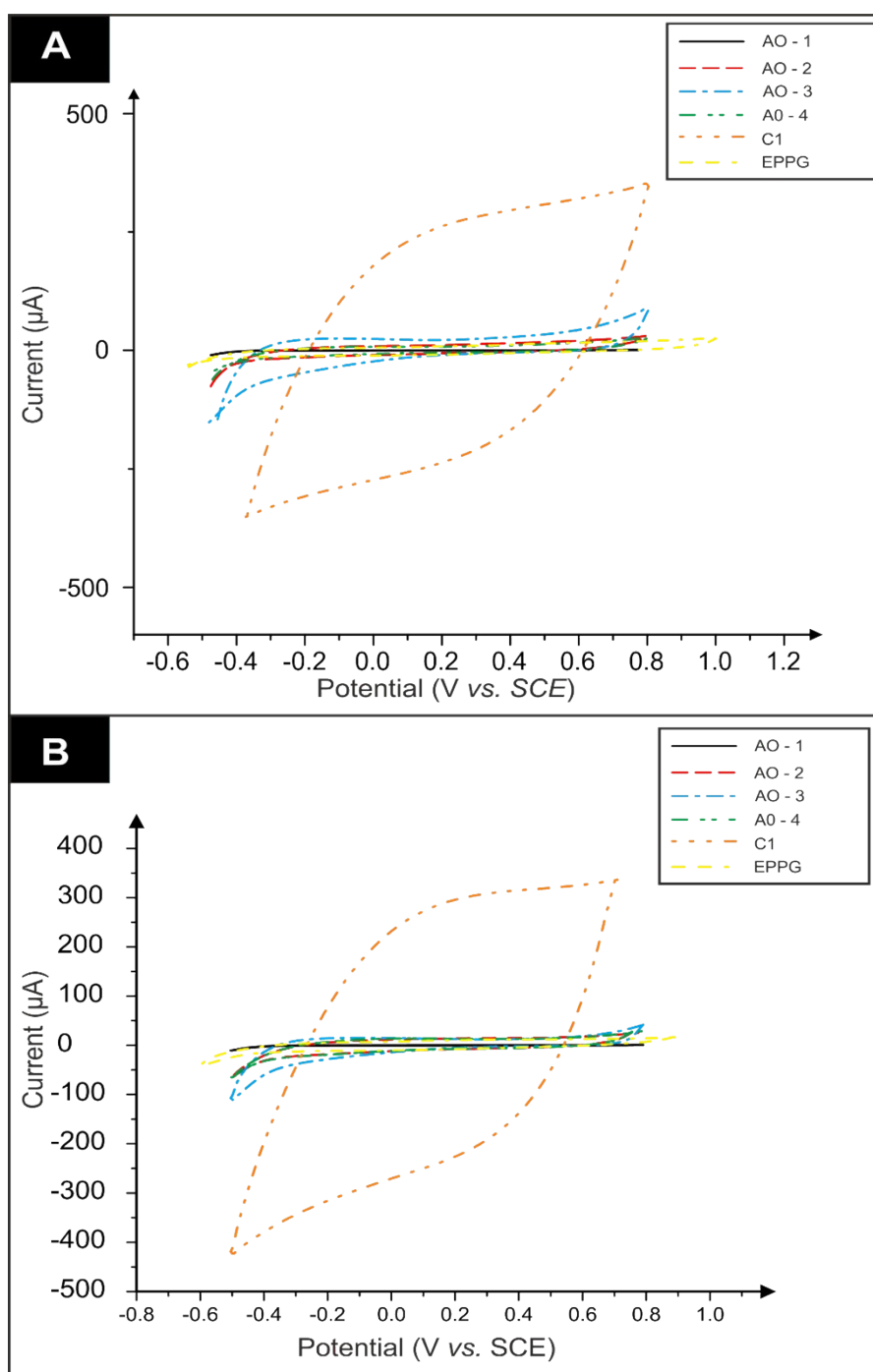
ESI Figure 15. XPS spectra showing the typical carbon responses of the commercially procured graphene powders; A) AO1, B) AO2, C) AO3 D) AO4 and E) C1.



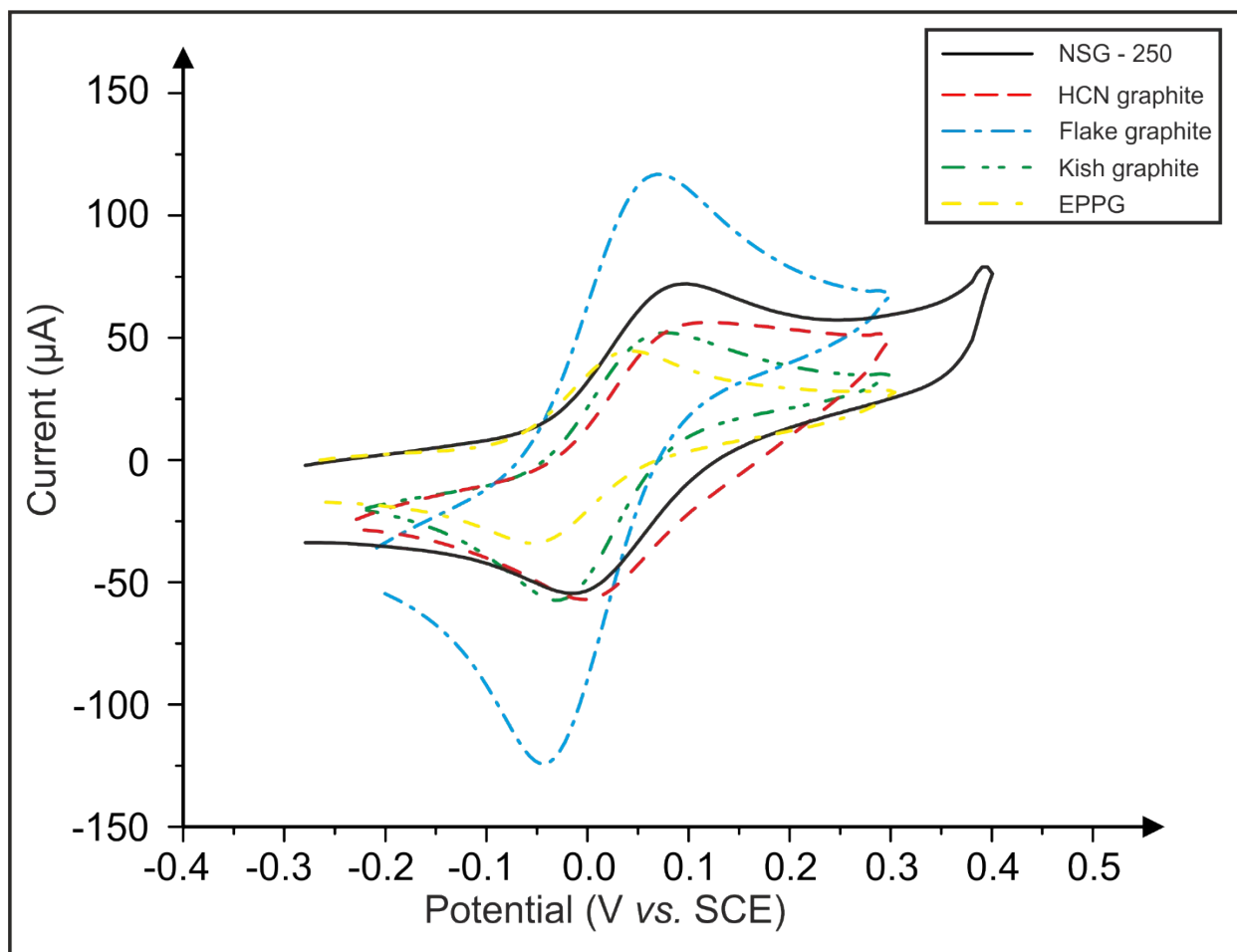
ESI Figure 16. Cyclic voltammetric profiles using the graphite paste electrodes towards a 0.1 M KCl control. A) Graphite paste electrodes during an anodic (oxidation) sweep. B) Graphite paste electrodes during a cathodic (reduction) sweep. These tests were performed in order to confirm that the oxidation and reduction peaks demonstrated throughout this study corresponded to the analytes used (redox probes). There are no observable peaks evident in the ‘blank’ tests and therefore this indicates that the analytes used throughout this study are responsible for the oxidation and reduction peaks produced. Scan rate: 100 mVs⁻¹.



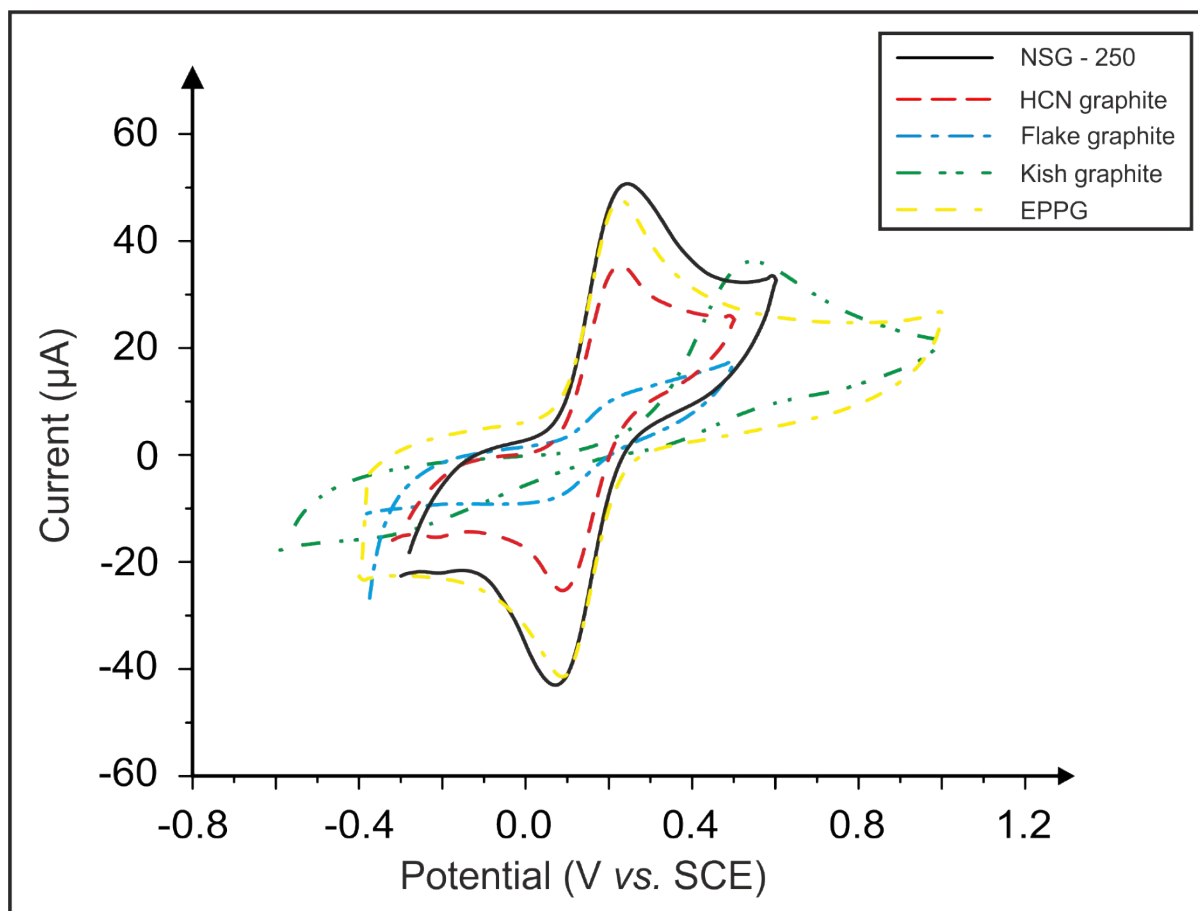
ESI Figure 17. Cyclic voltammetric profiles recorded in 0.1 M KCl when using the graphene paste electrodes. A) Graphene paste electrodes during an anodic (oxidation) sweep. B) Graphene paste electrodes during a cathodic (reduction) sweep. These tests were performed in order to confirm that the oxidation and reduction peaks demonstrated throughout this study corresponded to the analytes used (redox probes). There are no observable peaks evident and therefore this indicates that the analytes used throughout this study are responsible for the oxidation and reduction peaks produced. Scan rate: 100 mVs⁻¹.



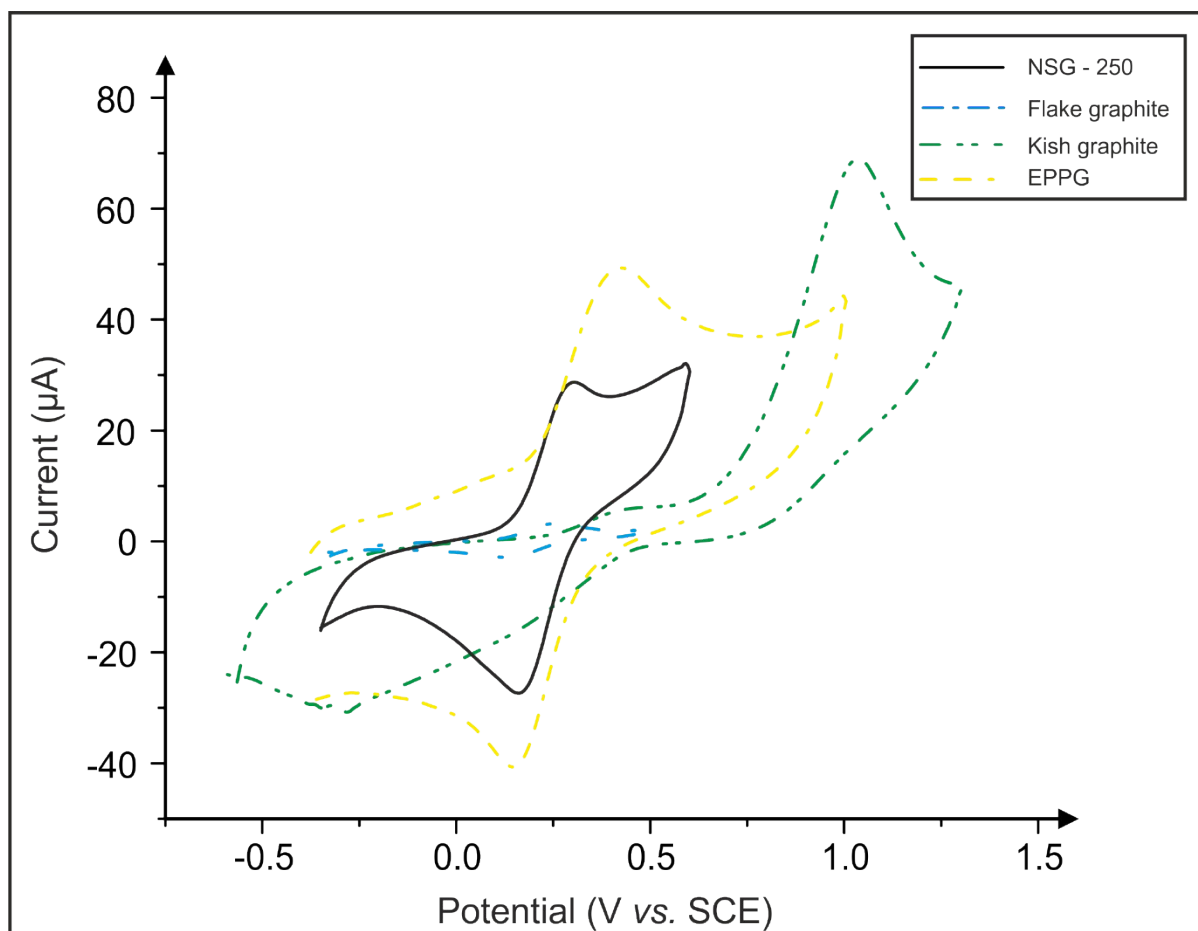
ESI Figure 18. Cyclic voltammetric profiles of the graphite paste electrodes recorded utilising 1 mM TMPD in 0.1 M KCl. Scan rate: 100 mVs⁻¹.



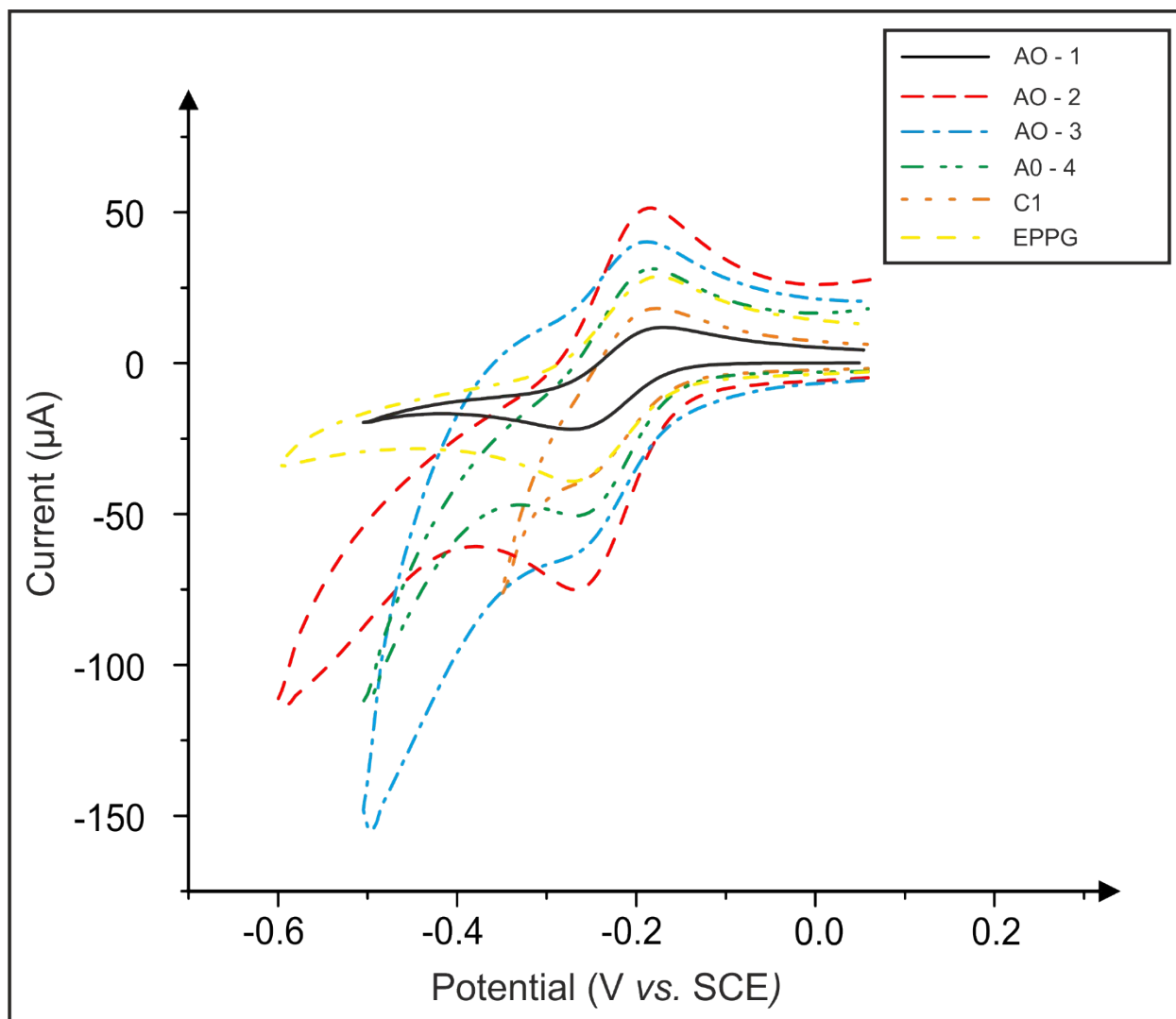
ESI Figure 19. Cyclic voltammetric profiles recorded using the graphite paste electrodes. Redox probe: 1 mM potassium ferrocyanide (II) / 0.1 M KCl. Scan rate: 100 mVs⁻¹.



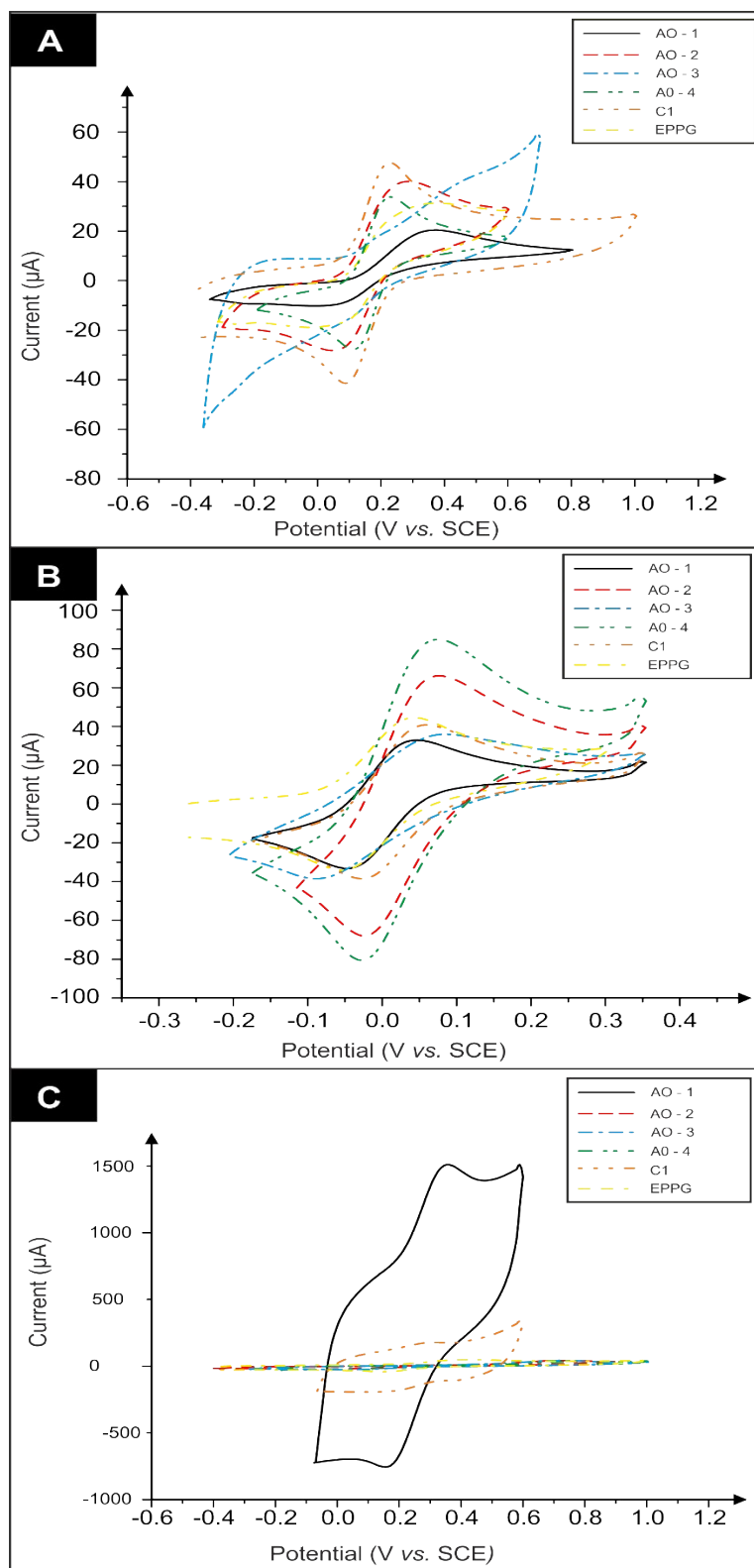
ESI Figure 20. Cyclic voltammetric profiles recorded using the graphite paste electrodes towards 1 mM ammonium ferrous(II)sulphate in 0.2 M perchloric acid. Scan rate: 100 mVs⁻¹. Note that this probe did not work well with High Crystalline Natural graphite, possibly due to oxygenated species found on the electrode surface.



ESI Figure 21. Cyclic voltammetric profiles recorded using the graphene paste electrodes. Redox probe: 1 mM Hexaammineruthenium(III) chloride / 0.1 M KCl. Scan rate: 100 mVs⁻¹.



ESI Figure 22. Cyclic voltammetric profiles of the graphene paste electrodes recorded utilising A) 1 mM TMPD in 0.1 M KCl, B) 1 mM potassium ferrocyanide (II) in 0.1 M KCl and C) 1 mM ammonium ferrous(II)sulphate in 0.2 M perchloric acid. Scan rate: 100 mVs⁻¹.



ESI Table 1. XPS analysis showing the chemical composition of the graphite powders. Unless otherwise stated, all tabulated values are reported in % Atomic Concentration.

| Chemical composition | Position / eV | Kish graphite | Flake graphite | High crystalline natural graphite | Nanostructured graphite - 250 |
|-----------------------------|----------------------|----------------------|-----------------------|--|--------------------------------------|
| C 1s | 284.5 | 90.30 | 88.60 | 97.50 | 96.20 |
| O 1s | 531.0 | 6.21 | 7.76 | 2.17 | 3.33 |
| Fe 2p | 711.5 | 0.19 | 0.54 | - | - |
| Si 2p | 101.0 | 2.18 | 2.57 | 0.33 | 0.27 |
| Al 2p | 75.5 | 0.43 | 0.57 | - | 0.15 |
| Cl 2p | 199.9 | 0.74 | - | - | - |

ESI Table 2. XPS analysis showing the chemical composition of the graphene powders. Unless otherwise stated, all tabulated values are reported in % Atomic Concentration.

| Chemical Composition | Position / eV | AO1 | AO2 | AO3 | AO4 | C1 |
|-----------------------------|----------------------|------------|------------|------------|------------|-----------|
| C 1s | 284.5 | 99.13 | 97.78 | 97.42 | 97.79 | 92.25 |
| O 1s | 531.0 | 0.73 | 2.22 | 2.40 | 2.12 | 6.27 |
| S 2p | 167.0 | 0.14 | - | 0.18 | 0.09 | - |
| Si 2p | 101.0 | - | - | - | - | 1.48 |

ESI Table 3. Porosity status of the graphite and graphene paste electrodes towards the hexaammineruthenium(III) chloride (0.1 M KCl) redox probe. For each of the paste electrodes noted, a semi-infinite linear diffusional response was evident, indicating results were based solely on diffusional processes, not due to surface adhesion.⁷

| Graphite used to fabricate paste electrode | Diffusional value calculated <i>via</i> the gradient of the log current (I_p) versus log scan rate (v) plot |
|---|---|
| Kish | 0.38 |
| Flake | 0.52 |
| High crystalline natural | 0.48 |
| Nanostructured – 250 | 0.50 |
| Graphene used to fabricate paste electrode | Diffusional value calculated <i>via</i> the gradient of the log current (I_p) versus log scan rate (v) plot |
| AO-1 | 0.37 |
| AO-3 | 0.59 |
| AO-4 | 0.50 |
| C1 | 0.45 |
| AO-2 | 0.52 |

ESI Table 4. Comparison of the electrochemical behaviour of the four graphitic electrodes towards the ammonium ferrous(II)sulphate probe (in 0.2 M perchloric acid). This redox probe was first characterised with an EPPG electrode and a ΔE_p of 256.81 mV was recorded ($N = 3$).

| Graphite type used to fabricate paste electrode | Average Measured Lateral Flake Size ($n = 20$) (μm) | ΔE_p (mV) – at 100 mV s⁻¹ |
|--|---|--|
| Kish graphite | 1389.9 (\pm 147.5) | 1027.2 (\pm 287.0) |
| Flake graphite | 608.0 (\pm 39.8) | 108.3 (\pm 7.4) |
| HCN graphite | 12.2 (\pm 0.7) | 229.9 (\pm 27.2) |
| Nanostructure graphite – 250 | 0.5 (\pm 0.1) | 136.0 (\pm 5.0) |

NB: Due to the lack of a coefficient value for ammonium ferrous(II)sulphate, it was not possible to deduce an average k^0 value or an area using an adapted Randles–Ševčík equation. Therefore, in this case, the values used for comparison will be the ΔE_p at 100 mV s⁻¹.

ESI Table 5. Comparison of the electrochemical behaviour at five graphene electrodes towards 1 mM TMPD (0.1 M KCl) ($N = 3$).

| Graphene type used to fabricate paste electrode | Average Measured Lateral Flake Size ($n = 20$) (μm) | k^0 (cm s^{-1}) | ΔE_p (mV) – at 100 mV s^{-1} |
|--|---|---|--|
| AO-1 | 9.4 (± 0.7) | 2.54×10^{-3} | 73.0 (± 2.1) |
| AO-3 | 5.0 (± 0.3) | 2.47×10^{-3} | 110.8 (± 4.6) |
| AO-4 | 4.0 (± 0.3) | 2.66×10^{-3} | 78.1 (± 2.1) |
| AO-2 | 2.3 (± 0.5) | 3.50×10^{-3} | 60.4 (± 0.1) |
| C1 | 1.3 (± 0.1) | 3.65×10^{-3} | 65.5 (± 1.4) |

ESI Table 6. Comparison of the electrochemical behaviour of five graphene electrodes towards 1 mM potassium ferrocyanide (II) (0.1 M KCl) ($N = 3$).

| Graphene type used to fabricate paste electrode | Average Measured Lateral Flake Size ($n = 20$) (μm) | k^0 (cm s^{-1}) | ΔE_p (mV) – at 100 mV s^{-1} |
|--|---|---|--|
| AO-1 | 9.4 (± 0.7) | 4.40×10^{-4} | 299.6 (± 14.4) |
| AO-3 | 5.0 (± 0.3) | 7.65×10^{-4} | 332.3 (± 24.7) |
| AO-4 | 4.0 (± 0.3) | 1.15×10^{-3} | 209.0 (± 18.5) |
| AO-2 | 2.3 (± 0.5) | 1.23×10^{-3} | 176.2 (± 0.1) |
| C1 | 1.3 (± 0.1) | 2.71×10^{-3} | 98.2 (± 2.1) |

ESI Table 7. Comparison of the electrochemical behaviour of the five graphene electrodes towards 1 mM ammonium ferrous(II)sulphate in 0.2 M perchloric acid. This redox probe was first characterised with an EPPG electrode and a ΔE_p of 256.8 mV was recorded ($N = 3$).

| Graphene type used to fabricate paste electrode | Average Measured Lateral Flake Size ($n = 20$) (μm) | ΔE_p (mV) – at 100 mV s^{-1} |
|--|---|--|
| AO-1 | 9.4 (± 0.7) | 153.6 (± 3.6) |
| AO-3 | 5.0 (± 0.3) | 752.8 (± 3.6) |
| AO-4 | 4.0 (± 0.3) | 662.2 (± 3.7) |
| AO-2 | 2.3 (± 0.5) | 737.7 (± 6.2) |
| C1 | 1.3 (± 0.1) | 68.0 (± 3.7) |

ESI Table 8. SEM-EDX analysis of the graphite and graphene flakes, showing average atomic percentage ($N = 3$).

| Elemental composition | Average Atomic Percentage (%) | | | | | | | | |
|-----------------------|-------------------------------|-------|-------|-------|-------|-------|-------|-------|----------------|
| | AO1 | AO2 | AO3 | AO4 | C1 | Kish | Flake | HCN | Nanostructured |
| Carbon | 91.33 | 96.75 | 95.50 | 96.20 | 96.43 | 96.25 | 88.23 | 96.85 | 96.20 |
| Oxygen | 4.56 | 3.01 | 4.27 | 3.18 | 3.03 | 3.45 | 10.62 | 2.88 | 3.56 |
| Silicon | 0.63 | 0.24 | 0.23 | 0.08 | 0.25 | 0.25 | 0.81 | 0.20 | 0.18 |
| Sodium | | | | 0.26 | | | | | |
| Sulphur | 1.02 | | | 0.19 | | | | | |
| Potassium | 2.32 | | | | | | | | |
| Aluminium | | | | 0.11 | 0.27 | 0.07 | 0.34 | 0.06 | 0.14 |
| Calcium | | | | 0.50 | | | | | |
| Magnesium | | | | | | | | 0.05 | 0.04 |

References

1. G. Wang, J. Yang, J. Park, X. Gou, B. Wang, H. Liu and J. Yao, *The Journal of Physical Chemistry C*, 2008, 112, 8192-8195.
2. J. Yan, T. Wei, B. Shao, F. Ma, Z. Fan, M. Zhang, C. Zheng, Y. Shang, W. Qian and F. Wei, *Carbon*, 2010, 48, 1731-1737.
3. K. Kakaei and M. Zhiani, *Journal of Power Sources*, 2013, 225, 356-363.
4. X. Li, J. Zhang, L. Shen, Y. Ma, W. Lei, Q. Cui and G. Zou, *Applied Physics A: Materials Science & Processing*, 2009, 94, 387-392.
5. E. Desimoni, G. Casella, A. Morone and A. Salvi, *Surface and Interface Analysis*, 1990, 15, 627-634.
6. C. Brundle, *Surface Science*, 1977, 66, 581-595.
7. D. A. C. Brownson, L. C. S. Figueiredo-Filho, X. Ji, M. Gomez-Mingot, J. Iniesta, O. Fatibello-Filho, D. K. Kampouris and C. E. Banks, *Journal of Materials Chemistry A*, 2013, 1, 5962-5972.
8. D. A. C. Brownson, D. K. Kampouris and C. E. Banks, *Chemical Society Reviews*, 2012, 41, 6944-6976.